

FEEDING AND FEEDBACK IN THE POWERFUL RADIO GALAXY 3C 120

F. TOMBESI^{1,2,3}, R. F. MUSHOTZKY², C. S. REYNOLDS², T. KALLMAN¹, J. N. REEVES⁴, V. BRAITO⁵, Y. UEDA⁶, M. A. LEUTENEGGER¹, B. J. WILLIAMS¹, L. STAWARZ⁷ AND M. CAPPI⁸

¹X-ray Astrophysics Laboratory, NASA/Goddard Space Flight Center, Greenbelt, MD 20771, USA; francesco.tombesi@nasa.gov

²Department of Astronomy, University of Maryland, College Park, MD 20742, USA; ftombesi@astro.umd.edu

³Dipartimento di Fisica, Università di Roma Tor Vergata, Via della Ricerca Scientifica 1, I-00133 Roma, Italy

⁴Astrophysics Group, School of Physical and Geographical Sciences, Keele University, Keele, Staffordshire, ST5 5BG, UK

⁵INAF - Osservatorio Astronomico di Brera, Via Bianchi 46 I-23807 Merate (LC), Italy

⁶Department of Astronomy, Kyoto University, Kyoto 606-8502, Japan

⁷Astronomical Observatory, Jagiellonian University, ul. Orla 171, 30-244, Kraków, Poland

and

⁸INAF-IASF Bologna, Via Gobetti 101, I-40129 Bologna, Italy

ABSTRACT

We present the spectral analysis of a 200 ks observation of the broad-line radio galaxy 3C 120 performed with the high energy transmission grating (HETG) spectrometer on board the *Chandra* X-ray Observatory. We find (i) a neutral absorption component intrinsic to the source with column density of $\log N_H = 20.67 \pm 0.05 \text{ cm}^{-2}$, (ii) no evidence for a warm absorber with an upper limit on the column density of just $\log N_H < 19.7 \text{ cm}^{-2}$ assuming the typical ionization parameter $\log \xi \simeq 2.5 \text{ erg s}^{-1} \text{ cm}$, the warm absorber may instead be replaced by (iii) a hot emitting gas with temperature $kT \simeq 0.7 \text{ keV}$ observed as soft X-ray emission from ionized Fe L-shell lines which may originate from a kpc scale shocked bubble inflated by the AGN wind or jet with a shock velocity of about $1,000 \text{ km s}^{-1}$ determined by the emission line width, (iv) a neutral Fe $K\alpha$ line and accompanying emission lines indicative of a Compton-thick cold reflector with low reflection fraction $R \simeq 0.2$, suggesting a large opening angle of the torus, (v) a highly ionized Fe XXV emission feature indicative of photoionized gas with ionization parameter $\log \xi = 3.75_{-0.38}^{+0.27} \text{ erg s}^{-1} \text{ cm}$ and a column density of $\log N_H > 22 \text{ cm}^{-2}$ localized within $\sim 2 \text{ pc}$ from the X-ray source, and (vi) possible signatures for a highly ionized disk wind. Together with previous evidence for intense molecular line emission, these results indicate that 3C 120 is likely a late state merger undergoing strong AGN feedback.

Keywords: black hole physics — line: identification — galaxies: active — X-rays: galaxies

1. INTRODUCTION

Increasing evidence points toward the possibility that virtually every galaxy hosts a supermassive black hole (SMBH) at its core, and that the evolution of both the

SMBH and the galaxy's baryonic component, i.e. stars and the intergalactic medium, may be intimately linked. The origin of this co-evolution is highly debated but it is likely that active galactic nuclei (AGN) may play an

important role through a process known as “feedback” (e.g., Silk & Rees 1998; Fabian 1999; Springel et al. 2005; Croton et al. 2006; Hopkins et al. 2008; Tombesi et al. 2015). Depending on whether the source is radio-quiet or radio-loud, the feedback is usually referred to as quasar/wind mode or radio/jet mode, respectively (e.g., Fabian 2012; King & Pounds 2015).

The dichotomy between radio-quiet and radio-loud AGN is still not fully understood, but it seems that the latter are more preferentially found in elliptical/disturbed galaxies and minor mergers (e.g., Xu, Livio & Baum 1999; Sikora, Stawarz & Lasota 2007; Chiaberge et al. 2015). The black hole spin may also play a role in driving the most powerful jets (e.g., Wilson & Colbert 1995; Hughes & Blandford 2003; Sikora, Stawarz & Lasota 2007; Garofalo, Evans & Sambruna 2010; Tchekhovskoy, Narayan & McKinney 2010). Moreover, the accumulation of magnetic flux near the black hole horizon has been suggested to play a role in the radio-loud/radio-quiet dichotomy as well (e.g., Tchekhovskoy, Narayan & McKinney 2011; Sikora & Begelman 2013). On the other hand, deeper observations, especially in the X-ray band, are showing that the differences in the central engines between the two classes of sources are rather subtle (Hardcastle et al. 2009; Tazaki et al. 2013; Bostrom et al. 2014).

Sensitive X-ray observations of radio galaxies show evidence for winds in this class of sources, similar to those observed in Seyferts, which are radio-quiet as a class (Tombesi et al. 2010a, 2013a; Gofford et al. 2013). Warm absorbers (WA) have been reported in 3C 382, 3C 445, 3C 390.3 and 4C+74.26 (Ballantyne 2005; Reeves et al. 2009, 2010; Torresi et al. 2010, 2012; Tombesi et al. 2016). Moreover, more extreme ultrafast outflows (UFOs) have also been reported in 3C 111, 3C 120, 3C 390.3, 3C 445, 4C+74.26, and Cygnus A (Tombesi et al. 2010b, 2011; Ballo et al. 2011; Braitto et al. 2011; Gofford et al. 2013; Reynolds et al. 2015). A recent X-ray study of a sample of 26 radio galaxies reported that the frequency of UFOs is likely in the interval $f \simeq (50 \pm 20)\%$ (Tombesi et al. 2014). Thus, contrary to the jet dichotomy, it seems that some type of winds may be present in both radio-quiet and radio-loud AGNs. Some of these winds may be powerful enough to provide a concurrent contribution to AGN feedback with jets (Tombesi et al. 2012a, b; Gofford et al. 2015).

Spectral features indicating reflection from the inner accretion disk and the parsec scale torus or broad line region have been reported in several radio galaxies as well (e.g., Kataoka et al. 2007; Sambruna et al. 2009; Tombesi et al. 2013b; Tazaki et al. 2013; Bostrom et al. 2014; Lohfink et al. 2015). Indeed, the presence of signatures of the accretion disk, winds, and jets in the composite broad-band spectra of broad-line radio

galaxies (BLRGs) make them the ideal objects to study the interplay among these components (e.g., Marscher et al. 2002; Chatterjee et al. 2009, 2011; Tombesi et al. 2011, 2012, 2013b; Lohfink et al. 2013; Fukumura et al. 2014; Clautice et al. 2016).

Here, we show the analysis of a long 200 ks *Chandra* high energy transmission grating (HETG) spectrometer observation of the radio galaxy 3C 120 ($z = 0.033$). This is the second paper on this series, the previous one was focused on the radio galaxy 3C 390.3 (Tombesi et al. 2016). The combined high energy resolution and moderate sensitivity in the wide energy band $E=0.5\text{--}7$ keV provided by the *Chandra* HETG spectrum are crucial for the detection of possible emission and absorption features from a wide range of ionization species, and it will provide one of the best high energy resolution spectrum of a radio galaxy to date.

The radio galaxy 3C 120 is particularly interesting for several different reasons: it has a borderline classification between FRI and FR II exhibiting a one-sided low inclination jet with bright X-ray knots (Harris et al. 2004), superluminal knots have been detected at parsec scales in the radio jet (Gómez et al. 2000), it has been detected in the γ -rays (Kataoka et al. 2011), it showed puzzling emission features in the soft X-rays (Petre et al. 1984; Torresi et al. 2012; Tombesi et al. 2014), its host galaxy is a disturbed S0 galaxy possibly the remnant of a minor merger, and it also shows significant molecular gas emission (Mazzarella et al. 1993; Evans et al. 2005). Therefore, this source may well represent a bridge between blazars, radio galaxies, Seyferts, and the final merger state of ultraluminous infrared galaxies (ULIRGs).

2. DATA REDUCTION AND ANALYSIS

Here, we describe the analysis of the *Chandra* HETG spectrum of the radio galaxy 3C 120. The observation is composed of four exposures performed within one month between December 2014 and January 2015 for a total exposure of about 200 ks, see Table 1 for details. No significant spectral variability is observed between the four exposures and the spectra are consistent with only $\simeq 3\%$ and $\simeq 10\%$ variations in photon index and source count rate, respectively.

The spectra were extracted using the *CIAO* package v4.7 and the associated CALDB. Only the first order dispersed spectra were considered for both the Medium Energy Grating (MEG) and High Energy Grating (HEG), and the ± 1 orders for each grating were subsequently combined for each sequence. The spectra from the separated exposures were combined to yield a single 1st order spectrum for each of the MEG and HEG gratings. The background count-rate is found to be always negligible. The resultant spectra were binned to the full width half

Table 1. Chandra HETG observations log for 3C 120.

Obs	ID	Date	Exp	Rate
1	16221	2014/12/19	78	0.82/0.40
2	17564	2014/12/22	30	0.77/0.38
3	17565	2014/12/27	43	0.53/0.26
4	17576	2015/01/27	43	0.82/0.41

NOTE—Columns: observation number; observation ID; observation date; exposure in ks; MEG/HEG count rates.

maximum (FWHM) of their spectral resolution, which corresponds to $\Delta\lambda = 0.023 \text{ \AA}$ and $\Delta\lambda = 0.012 \text{ \AA}$ bins for MEG and HEG, respectively. The MEG and HEG spectra were analyzed in the energy bands $E=0.5\text{--}7 \text{ keV}$ and $E=1\text{--}7.5 \text{ keV}$, respectively. The analysis of the background subtracted source spectra was performed using *XSPEC* v.12.8.2 and the C-statistic was applied. We performed simultaneous fits of the MEG and HEG spectra allowing a free cross-normalization constant, whose fitted value was always consistent with unity. All parameters are given in the source rest frame and the errors are at the 1σ level if not otherwise stated. Standard Solar abundances are assumed (Asplund et al. 2009).

2.1. Phenomenological spectral analysis of 3C 120

We started the spectral analysis including a continuum power-law with $\Gamma \simeq 1.7$ ($C/\nu = 2407/2220$). A Galactic absorption of $N_H = 1.1 \times 10^{21} \text{ cm}^{-2}$ modeled with *wabs* in *XSPEC* is included in all the fits (Kalberla et al. 2005). Equivalent results are obtained using the *TBabs* model in *XSPEC*. An inspection of the data in Fig. 1 show the possible presence of absorption residuals in the soft X-rays and possible emission lines. Indeed, an additional neutral absorber intrinsic to the source with column density of $N_H = (4.3 \pm 0.5) \times 10^{20} \text{ cm}^{-2}$ is highly required ($\Delta C/\Delta\nu = 81/1$). Equivalent results are obtained using either *zwabs* or *zTBabs* models in *XSPEC*.

2.1.1. Emission lines in the soft X-ray band

In Fig. 2 we can see a series of possible emission features in the energy range between $E=0.65\text{--}0.85 \text{ keV}$. When modeled with Gaussian emission lines, the rest-frame energies of the two most significant features are at $E=719 \pm 3 \text{ eV}$ and $E=777_{-7}^{+2} \text{ eV}$, respectively. The parameters of the lines are reported in Table 2. We consider only the lines with a fit improvement of $\Delta C \geq 4$ for two additional degrees of freedom, corresponding to a detection significance higher than 90%.

The $E \simeq 719 \text{ eV}$ feature is relatively broad, with a

width of $\sigma = 8 \pm 2 \text{ eV}$. The closest lines¹ to the first emission feature is the ionized Fe L-shell doublet of Fe XVII, with transitions respectively at the energies of $E=727 \text{ eV}$ and $E=739 \text{ eV}$. Another spectral feature close to the observed energy is O VII radiative recombination continuum (RRC) at $E=739 \text{ eV}$ (e.g., Liedahl & Paerels 1996). The only other features around this energy are the $L\alpha$ and $L\beta$ fluorescence lines from neutral or lowly ionized Fe at $E=705 \text{ eV}$ and $E=719 \text{ eV}$, respectively. The possible alternative interpretations of this feature are discussed in the following section using more physical models.

The second emission line at the energy of $E=777 \text{ eV}$ may be associated with the Fe XVIII $2p \rightarrow 3s$ doublet at $E=777 \text{ eV}$ and $E=779 \text{ eV}$, or with O VIII $L\gamma\beta$ at $E=775 \text{ eV}$. The latter possibility is supported by the detection of O VIII $L\gamma\alpha$ at $E \simeq 650 \text{ eV}$ in the *XMM-Newton* reflection grating spectrometer (RGS) spectrum (Ogle et al. 2005; Torresi et al. 2012). The *XMM-Newton* RGS provided better signal-to-noise data at energies below $E \simeq 700 \text{ eV}$, while *Chandra* HETG is superior at higher energies.

2.1.2. Emission lines in the Fe K band

In Fig. 3 we show the ratio between the data and the absorbed power-law continuum in the Fe K region between $E=5.5\text{--}7.5 \text{ keV}$. We note the presence several emission features.

The emission line at the energy of $E=6394 \pm 5 \text{ eV}$ is detected with very high significance ($\Delta C/\Delta\nu = 40/2$), and it is clearly identified with the Fe $K\alpha$ fluorescence emission doublet from neutral or lowly ionized material ($K\alpha_1$ at $E=6391 \text{ eV}$ and $K\alpha_2$ at $E=6404 \text{ eV}$). The emission line at $E=6232_{-23}^{+8} \text{ eV}$, even though less significant, is at the exact energy expected for the Compton shoulder of the main Fe $K\alpha$ line of $E \simeq 6240 \text{ eV}$ (e.g., Matt 2002; Watanabe et al. 2003; Yaqoob & Murphy 2011).

¹ The line identifications are derived from the National Institute of Standards and Technology (NIST) database or Verner et al. (1996).

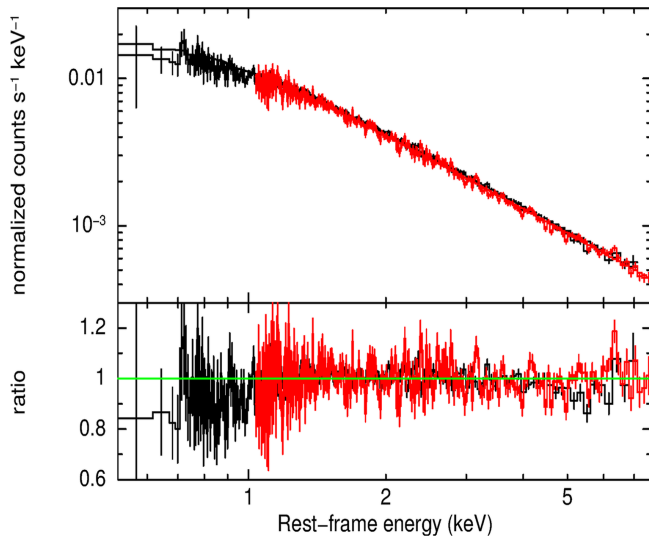


Figure 1. Combined *Chandra* MEG (black) and HEG (red) spectra of 3C 120 compared to a Galactic absorbed power-law continuum model. *Upper panel:* spectra and continuum model, the data are divided by the response effective area for each channel. *Lower panel:* data to model ratio. We note the presence of soft X-ray absorption residuals and several emission lines. The data are binned to $4\times$ the FWHM resolution and to a minimum signal-to-noise of 5 for clarity.

The emission line at $E=7055_{-15}^{+21}$ eV is instead at the energy consistent with the accompanying Fe K β fluorescence line at $E=7058$ eV. If this interpretation is correct, then the equivalent width of this feature is estimated to be $\simeq 60\%$ of the K α . This is much larger than the typical value of $\simeq 11\%$ expected for the K β from atomic physics (e.g., George & Fabian 1991). One possible explanation for this discrepancy could be that the K β line is blended with other features. The closest emission feature would be Fe XXVI Ly α at energy of $E=6970$ eV. However, this possibility seems unlikely because the K β line is unresolved.

The Fe K β /Fe K α ratio of emission line photons that escape from the obscuring torus may be higher than the tabulated value when the medium is optically thick to absorption of either of the two emission lines. This is due to the differential absorption opacities for the Fe K α and Fe K β lines. Moreover, possible clumpiness in the torus may affect this ratio. In the next section we explore more physically motivated models for these features and discuss a possible interpretation for the discrepancy in the equivalent width ratio.

The emission feature at $E=6703_{-20}^{+5}$ eV is consistent with the energy of the Fe XXV He α resonance emission line at $E=6700$ eV. A similar feature was observed also in lower energy resolution spectra from *Suzaku* and *XMM-Newton* (e.g., Tombesi et al. 2010b, 2014; Lohfink et al. 2013; Gofford et al. 2013). The limited signal-to-noise and bandwidth in the Fe K region of the present *Chandra* HETG spectrum does not allow to detect the

broad Fe K emission feature previously reported in a *Suzaku* observation (Kataoka et al. 2007). The parameters of the lines are reported in Table 2.

2.2. Spectral analysis of 3C 120 with physical models

After the initial phenomenological modeling, we performed a more physically motivated fit of the spectrum. The starting model was an absorbed power-law.

2.2.1. Emission lines in the Fe K band

We replaced the Fe K α emission line in turn with a cold reflection component *peaxmon* (Nandra et al. 2007), and an ionized reflection component *xillver* (Garcia et al. 2014). We assumed an inclination angle of 20° consistent with the radio jet (Jorstad et al. 2005), a standard Solar abundance for iron and a high energy cut-off of $E=300$ keV as estimated from hard X-ray observations (e.g., Kataoka et al. 2007; Tombesi et al. 2014). The *peaxmon* reflection component also includes the Fe K α and K β emission lines at $E=6.4$ keV and $E=7.058$ keV with equivalent width ratio of 11%, and the Ni K α at $E=7.470$ keV with a flux of $\simeq 5\%$ of the Fe K α .

The Compton shoulder of the Fe K α line, denoted as Fe K α_c , is included in *peaxmon*, but it is only roughly approximated as a Gaussian emission line at the energy $E=6.315$ keV, with width $\sigma=35$ eV, and equivalent width (EW) following the prescription of Matt (2002). This may be a reasonable approximation for low resolution spectra, in which the line and Compton shoulder are blended together, but it may be not adequate for the high resolution *Chandra* HETG data discussed here.

An initial fit comparing *peaxmon* to *xillver* shows that the former component is preferred, giving a reflection fraction of $R = 0.22 \pm 0.04$. The reflection fraction is defined as $R = \Omega/2\pi$, where Ω is the solid angle of the reflector. This is consistent with previous broad-band analyses (e.g., Kataoka et al. 2007; Tombesi et al. 2014). The statistical improvement of the inclusion of the *peaxmon* component with respect to the absorbed power-law continuum is very high, $\Delta C/\Delta \nu = 47/1$. There is no requirement for broadening of this component, consistent with the fact that the Fe K α line is unresolved ($\sigma_E < 20$ eV) and likely due to material relatively distant from the SMBH. The alternative modeling with a *xillver* component provides a lower statistical improvement ($\Delta C/\Delta \nu = 38/2$), with an upper limit on the ionization parameter of $\log \xi < 0.8$ erg s $^{-1}$ cm, again consistent with lowly ionized or neutral material.

In order to derive a proper modeling of the Fe K α emission line, the associated Fe K β , and Compton shoulder, we replaced *peaxmon* using the more detailed torus reflection model *MYTorus* (Murphy & Yaqoob 2009; Yaqoob & Murphy 2011). The main parameters of this model are the power-law slope, assumed to be the

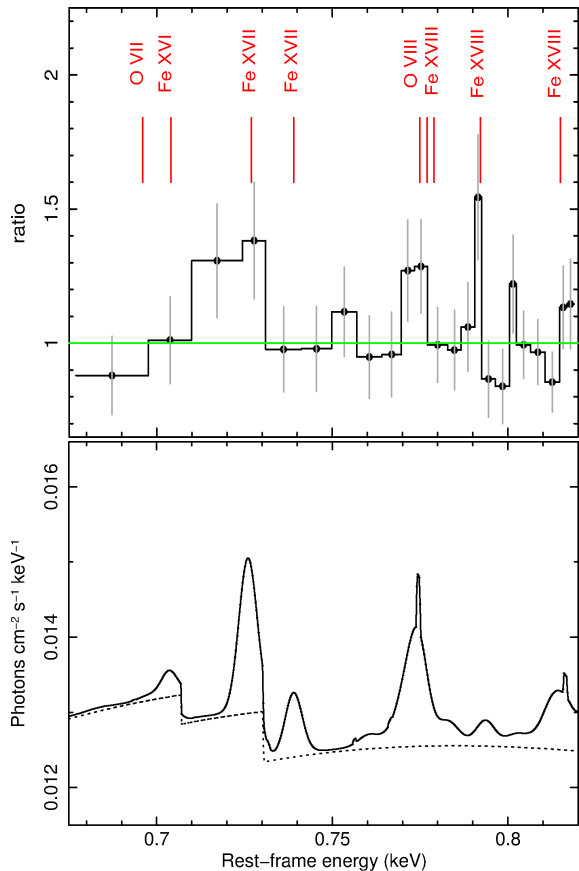


Figure 2. *Upper panel:* data to model ratio of the *Chandra* MEG spectrum of 3C 120 in the $E=0.65\text{--}0.85$ keV energy band with respect to a Galactic absorbed power-law continuum model. The data are binned to $2\times$ the FWHM resolution and a minimum signal-to-noise of 5 for clarity. The vertical lines indicate the possible identifications. *Lower panel:* best-fit model including a hot emission component for the soft X-ray lines. The dotted line indicates the absorbed continuum.

same as the power-law continuum, the inclination angle, assumed to be $\theta=20^\circ$ from the radio jet (Jorstad et al. 2005), and the torus column density. The inclusion of this component provides a very good fit, with a statistical improvement of $\Delta C/\Delta\nu = 45/1$. The column density is estimated to be $N_H > 6 \times 10^{24} \text{ cm}^{-2}$ at the 90% level. Even if this fit is statistically comparable to the one using *peaxmon*, in the following we will use *MYTorus* because it provides a more physically self-consistent treatment of the X-ray reflection from cold distant material in a toroidal configuration.

The ratio between the Fe $K\alpha$ and the Compton shoulder $C = (0.1 + 0.1\cos\theta)$ depends on the inclination of the system θ (e.g., Matt 2002). Considering an inclination consistent with the one of the radio jet of $\theta = 20.5^\circ \pm 1.8^\circ$ (Jorstad et al. 2005) and the $\text{EW} \simeq 32$ eV of the Fe $K\alpha$ line from Table 2, we estimate an EW of the Compton shoulder of $\text{EW} \simeq 7$ eV which is consistent with the observed value. Given the low inclination of 3C 120,

the $\text{EW} \simeq 30$ eV of the Fe $K\alpha$ suggests a high column density of $N_H > 1 \times 10^{24} \text{ cm}^{-2}$ for the torus, which is outside of our line of sight. This is supported by the detection of the Compton shoulder, which indicates a toroidal structure with a column density of the order of $N_H > 6 \times 10^{24} \text{ cm}^{-2}$ from the best-fit using *MYTorus*.

Considering the torus reflection model developed by Ikeda et al. (2009) and the calculations reported in Fig. 7 of Tazaki et al. (2013) assuming the parameters estimated for 3C 120, i.e., an Fe $K\alpha$ line with $\text{EW} \simeq 30$ eV, an inclination angle of $\simeq 20^\circ$, and a torus column density of $N_H \simeq 1 \times 10^{24} \text{ cm}^{-2}$, we derive that the torus should have a large opening angle of $> 80^\circ$ and therefore a small covering fraction. The main difference between the torus model by Ikeda et al. (2009) and *MYTorus* is geometrical, with the former assuming an almost spherical geometry with coneshaped bipolar holes, whose opening angle is a free parameter, and a fixed torus-like geometry for the latter. We note that we do not observe absorption from the torus even if it is likely Compton-thick due to the large opening angle of the torus and low inclination angle of the disk/jet along our line of sight.

The ionized emission line at $E=6.7$ keV can be well modeled including an *xstar* photo-ionized emission component (Kallman & Bautista 2001). We calculated an *xstar* emission table considering a power-law continuum of $\Gamma = 1.7$. The free parameters of this model are the ionization parameter, the column density, and the normalization. The normalization is defined as $N = fL_{\text{ion}}/D^2$, where $f = \Omega/4\pi$ is the covering fraction of the material, L_{ion} is the ionizing luminosity in units of $10^{38} \text{ erg s}^{-1}$ from 1 (1 Ryd = 13.6 eV) to 1,000 Ryd, and D is the distance of the observer to the source in kpc. The emitter normalization and column density are degenerate. By assuming a covering fraction $f=1$ we can derive a lower limit for the column density. Substituting the appropriate values of distance² $D \simeq 1.35 \times 10^5$ kpc for 3C 120 and the absorption corrected ionizing luminosity of $L_{\text{ion}} \simeq 3.8 \times 10^6 (\times 10^{38}) \text{ erg s}^{-1}$ extrapolated from the best-fit model, we obtain an estimate for the normalization of $N \simeq 2 \times 10^{-4}$. The inclusion of this component is required with a significance of 99% ($\Delta C/\Delta\nu = 9/2$). The resultant ionization parameter is high, $\log\xi = 3.75^{+0.27}_{-0.38} \text{ erg s}^{-1} \text{ cm}$. The ionization parameter is defined as $\xi = L_{\text{ion}}/nr^2 \text{ erg s}^{-1} \text{ cm}$ (Tarter, Tucker & Salpeter 1969) where n is the number density of the material, and r is the distance of the gas from the central source. We can also estimate a lower limit for the column density of $N_H > 1 \times 10^{22} \text{ cm}^{-2}$. Even after including the cold reflection and photo-ionized emission

² Assuming cosmological parameters $H_0 = 73.00 \text{ km sec}^{-1} \text{ Mpc}^{-2}$, $\Omega_{\text{matter}} = 0.27$, $\Omega_{\text{vacuum}} = 0.73$

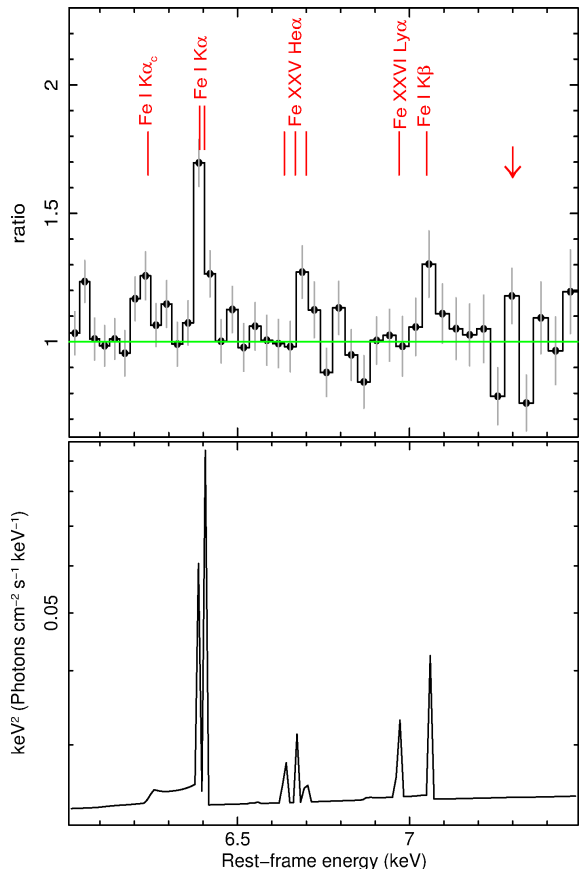


Figure 3. *Upper panel:* data to model ratio of the *Chandra* HEG spectrum of 3C 120 in the E=5–7.5 keV energy band with respect to a Galactic absorbed power-law continuum model. The data are binned to the FWHM resolution. The vertical lines indicate the expected energies of the major Fe K transitions. The vertical arrow indicates the possible blue-shifted Fe K absorption residuals. *Lower panel:* best-fit model including emission from cold reflection and photoionized gas.

components we find that there is still a marginally significant excess of emission at the energy of the neutral Fe K β fluorescence line. The best-fit model is shown in the lower panel of Fig. 3.

2.2.2. Emission lines in the soft X-rays

We tested several models to explain the soft X-ray emission lines. We started by including a collisional ionization component using the *apec* model (Smith et al. 2001). We also included a Gaussian broadening given that the line was resolved. In this case the line would be interpreted as emission from Fe XVII Ly α and slightly lower ionization species. The best-fit parameters are a broadening of $\sigma=2.7^{+2.6}_{-0.1}$ eV, a temperature of $kT=0.4^{+0.3}_{-0.1}$ keV and a normalization of $N=(2.1^{+1.5}_{-1.0}) \times 10^{-4}$. The fit improvement is $\Delta C/\Delta\nu=10/3$.

We considered also a non-equilibrium ionization collisional plasma model, *nei* in *XSPEC*. This model allows to approximate the condition in shocks or hot plasmas and is applicable also to supernova remnants

(e.g., Borkowski, Lyerly & Reynolds 2001). This provides a higher fit improvement of $\Delta C = 13/3$ compared to a simple *apec* model. We estimate a broadening of $\text{FWHM}=2,400^{+1,400}_{-1,800}$ km s $^{-1}$, a temperature of $kT=(0.7^{+0.9}_{-0.1})$ keV, an ionization timescale of $\tau=(1.3^{+1.2}_{-1.0}) \times 10^{11}$ s cm $^{-3}$ and a normalization of $N=(1.2^{+0.6}_{-0.8}) \times 10^{-4}$. Equivalent results are obtained using the plane-parallel shocked plasma model *pshock* in *XSPEC*.

The normalization of both the *apec* and *nei* models in *XSPEC* is defined as $N = 10^{-14}(EM/4\pi[D_A(1+z)]^2)$, where $D_A \simeq 3.9 \times 10^{26}$ cm is the angular diameter distance to 3C 120. The emission measure EM is defined as $EM = \int n_e n_H dV$, where n_e and n_H are the electron and hydrogen number densities in cm $^{-3}$, respectively. Given the normalization of the *nei* component, we can estimate an emission measure of $EM = 2 \times 10^{68} N = (2.4^{+1.2}_{-1.6}) \times 10^{64}$ cm $^{-3}$.

We also investigated the possible interpretation of the emission lines as due to a photo-ionized component using the *xstar* model. We assume the same *xstar* emission table used for the Fe K band, considering a power-law continuum of $\Gamma = 1.7$ and turbulence velocity of 100 km s $^{-1}$. We also considered a normalization of $N \simeq 2 \times 10^{-4}$ consistent with the source parameters assuming a covering fraction of unity.

The inclusion of this component provides a lower fit improvement compared to the previous ones of $\Delta C/\Delta\nu=7/2$. The best-fit ionization parameter is $\log \xi=2.15^{+0.17}_{-0.24}$ erg s $^{-1}$ cm, and the lower limit on the column density is $N_H > 1 \times 10^{20}$ cm $^{-2}$, respectively. In this case the feature at the energy of E \sim 777 eV would be interpreted as O VIII He β . However, this modeling does not provide an adequate characterization of the emission feature at E \sim 719 eV because in this case the closest feature would only be O VII RRC at E \simeq 739 eV.

We note that similar soft X-ray features were also reported in the *XMM-Newton* RGS spectrum of 3C 120 performed by Torresi et al. (2012). The authors tested two possible scenarios: Fe XVII from a collisionally ionized gas or O VII RRC from a photoionized gas. Torresi et al. (2012) concluded that the limited signal-to-noise and complexity of the data could not favor neither one of these two possibilities, leaving the origin of the emitting gas as an open question. Moreover, Tombesi et al. (2014) reported the detection of an excess emission in the soft X-ray band using *Suzaku*, but the feature was phenomenologically parameterized with a simple black-body component with a temperature $kT \simeq 0.4$ keV given the insufficient energy resolution of that detector.

Finally, we tested an alternative interpretation of the soft X-ray emission lines as due to L-shell fluorescence from neutral or slightly ionized Fe. Fe L-shell flu-

Table 2. Best-fit parameters of the emission lines in 3C 120.

E	σ	I	EW	ID	ΔC
soft X-ray emission lines					
719 ± 3	8 ± 2	23.0 ± 8.0	8 ± 2	Fe XVII	12
777_{-7}^{+2}	$< 50^a$	5.8 ± 3.4	2 ± 1	Fe XVIII/O VIII	5
Fe K emission lines					
6232_{-23}^{+8}	$< 330^a$	$0.5_{-0.2}^{+0.3}$	8 ± 4	Fe K α_c	6
6394 ± 5	$< 20^a$	1.9 ± 0.3	32 ± 6	Fe K α	40
6703_{-20}^{+5}	$< 40^a$	$0.6_{-0.2}^{+0.4}$	11 ± 5	Fe XXV He α	6
7055_{-15}^{+21}	$< 80^a$	1.0 ± 0.4	20_{-8}^{+6}	Fe K β	9

^a90% upper limit.

NOTE—Columns: rest-frame energy in eV; line width in eV; intensity in units of 10^{-5} ph s $^{-1}$ cm $^{-2}$; EW in eV; line identification; C-statistics improvement after including the Gaussian line. The line identifications are derived from the National Institute of Standards and Technology (NIST) database at www.nist.gov, Verner et al. (1996) and Kaye & Laby at www.kayelaby.npl.co.uk.

orescence lines would be expected at the energies of E=705 eV, E=719 eV, and E=792 eV, which are roughly consistent with the observed features.

Although this being an intriguing possibility, when we consider a physical model for the reflection off cold material such as *peaxmon* or *MYTorus* we note that the low energy photons are drastically affected by photoelectric absorption from the same medium that should give rise to the Fe L lines. Therefore, neutral Fe L fluorescence features would be undetectable in this physical scenario.

Instead, Fe L-shell resonance emission lines may be more intense if we consider lowly or mildly ionized reflection. In the previous section we discussed a fit using the *xillver* model which can provide a relatively good modeling of the Fe K line with very low ionization $\log\xi < 0.8$ erg s cm $^{-1}$. However, checking the region around E=0.7–0.75 keV we find no detectable features from the model because ionized Fe L-shell resonance lines, along with many others unobserved fea-

Absorption lines indicative of ultrafast outflows in the Fe K band have been reported in two *Suzaku* observations of 3C 120 performed in 2006 and 2012 (Tombesi et al. 2010b, 2014). The outflow in the 2006 *Suzaku* observation was detected in the energy range between E \simeq 7–7.3 keV with velocity $v_{out} \simeq 0.08c$, ionization parameter $\log\xi \simeq 3.8$ erg s $^{-1}$ cm and column density $N_H \simeq 1 \times 10^{22}$ cm $^{-2}$ (Tombesi et al. 2010b). The 2012 observation showed an outflow at the energy of E \simeq 7.7 keV with higher velocity and ionization, i.e., $v_{out} \simeq 0.16c$, $\log\xi \simeq 4.9$ erg s $^{-1}$ cm and $N_H > 2 \times 10^{22}$ cm $^{-2}$ (Tombesi et al. 2014).

The signal-to-noise and limited high-energy bandwidth of the *Chandra* HETG are not adequate to clearly

tures, would show up only for much higher ionization levels around $\log\xi \sim 2$ erg s cm $^{-2}$.

Therefore, an origin of the prominent emission feature at E \sim 0.7–0.75 keV from hot gas is preferred over fluorescence, photoionization, and ionized reflection. The best-fit model is shown in the lower panel of Fig. 2.

2.2.3. Absorption in the soft X-ray and Fe K bands

We performed a search for possible absorption features in both the soft X-rays and in the Fe K band. In the soft X-ray band we do not find absorption lines with a statistical significance higher than 99% indicating that, if present, the WA is either highly ionized or it has a low column density. This is consistent with previous studies using *XMM-Newton* RGS (Ogle et al. 2005; Torresi et al. 2012). Using an *xstar* photo-ionized absorption table and assuming the typical ionization of the WA detected in other BLRGs of $\log\xi \simeq 2.5$ erg s $^{-1}$ cm (Reeves et al. 2009; Torresi et al. 2010, 2012) we estimate an upper limit of the column density of just $N_H < 5 \times 10^{19}$ cm $^{-2}$. detect such features. Nonetheless, in Fig. 3 there is a hint for absorption features in the energy range between E \simeq 7.2–7.4 keV. We checked for the presence of an outflow using an *xstar* photo-ionization table with an input power-law continuum slope of $\Gamma=1.7$ and a turbulence velocity of 1,000 km s $^{-1}$. We find that an outflow may be present at the 99% level using the F-test ($\Delta C/\Delta\nu=11/3$). However, we note that the significance may be lowered down to about 90–95% considering a blind line search between E=7.0–7.5 keV, which corresponds to about 10 intervals at the HEG resolution of 50 eV. The best-fit indicates an outflow velocity of $v_{out}=0.068 \pm 0.002c$, ionization parameter $\log\xi=3.48_{-0.10}^{+0.17}$ erg s $^{-1}$ cm, and column density

$N_H = (3.3_{-1.6}^{+2.4}) \times 10^{21} \text{ cm}^{-2}$. These parameters would suggest the presence of an ultrafast outflow with characteristics similar to the one detected in the 2006 *Suzaku* observation (Tombesi et al. 2010b, 2014). The final best-fit model is shown in Fig. 4 and the parameters are listed in Table 3.

3. DISCUSSION

The analysis of the *Chandra* HETG spectrum of 3C 120 reveals a rather complex multi-phase and multi-scale environment in this radio galaxy. In the following we will describe a physical interpretation for each component.

3.1. Emission in the soft X-rays

The soft X-ray band of 3C 120 below $E \simeq 1$ keV is rather complex and the current *Chandra* data show a series of emission lines in the energy range between $E \simeq 0.6$ – 0.9 keV.

The first report of possible thermal emission lines in the soft X-ray spectrum of 3C 120 was published by Petre et al. (1984) using *Einstein* Observatory data. The excess emission between $E = 0.5$ – 2 keV was modeled with a thermal bremsstrahlung component with temperature near 1 keV. The signature of this component was the presence of weak emission lines at energies consistent with Fe L, Mg K, and Si K. Similar soft X-ray structures were also reported in the *XMM-Newton* and *Suzaku* spectra of 3C 120 (Torresi et al. 2012; Tombesi et al. 2014). The most intense of these features are likely associated with ionized Fe L transitions.

We tested several different alternatives for the origin of the emission in the soft X-rays and found that a non-equilibrium ionization collisional plasma model with an electron temperature of $kT = (0.7_{-0.1}^{+0.9})$ keV provides both the best-fit and a physically plausible explanation. This model allows to approximate the condition in shocks or hot plasmas.

The fact that the data require a broadening of this hot emission component indicates that there is an additional component compared to just the thermal one, that for this $T \simeq 10^7$ K plasma would be only $v_{th} = \sqrt{2kT/m_{Fe}} \simeq 50 \text{ km s}^{-1}$. Instead, the width of the emission component is much larger and corresponds to a velocity broadening of $\text{FWHM} = 2,400_{-1,800}^{+1,400} \text{ km s}^{-1}$. This additional velocity component could be either associated a spherical outflow or an expanding spherical shock. We note that this velocity is much higher than just the thermal broadening or turbulence from hot interstellar medium, being both typically less than 100 km s^{-1} (Werner et al. 2009).

Table 3. Best-fit model of the *Chandra* HETG spectrum of 3C 120.

Power-law continuum	
Γ	1.771 ± 0.008
Neutral abs	
$\log N_H \text{ (cm}^{-2}\text{)}$	20.67 ± 0.05
Gsmooth \times nei emission	
FWHM (10^3 km s^{-1})	$2.4_{-1.8}^{+1.4}$
kT (keV)	$0.7_{-0.1}^{+0.9}$
$\tau \text{ (} 10^{11} \text{ s cm}^{-3}\text{)}$	$1.3_{-1.0}^{+1.2}$
EM (10^{64} cm^{-3})	$2.4_{-1.6}^{+1.2}$
MYTorus	
θ (deg)	20
$\log N_H \text{ (cm}^{-2}\text{)}$	$> 24.8^*$
Xstar emission	
$\log \xi \text{ (erg s}^{-1} \text{ cm)}$	$3.75_{-0.38}^{+0.27}$
$N_H \text{ (} 10^{21} \text{ cm}^{-2}\text{)}$	$> 10^*$
Xstar absorption	
$\log \xi \text{ (erg s}^{-1} \text{ cm)}$	$3.48_{-0.10}^{+0.17}$
$N_H \text{ (} 10^{21} \text{ cm}^{-2}\text{)}$	$3.3_{-1.6}^{+2.4}$
$v_{out} \text{ (c)}$	0.068 ± 0.002
C-statistic	
C/ν	2256/2209
Flux ^a	
0.5–2 keV	3.4
2–7 keV	4.1

^aIntrinsic power-law continuum flux in units of $10^{-11} \text{ erg s}^{-1} \text{ cm}^{-2}$

*90% lower or upper limit.

We estimate an emission measure of $EM = (2.4_{-1.6}^{+1.2}) \times 10^{64} \text{ cm}^{-3}$. Values of the emission measure of the order of 10^{64} cm^{-3} have also been reported also for the hot interstellar medium observed through Fe XVII emission at temperatures of $kT \leq 0.8$ keV in the cores of large elliptical galaxies (Werner et al. 2009). Considering the emission measure and assuming a fully ionized plasma, $n_e \simeq 1.2n_H$, and considering a roughly spherical volume of radius ~ 1.3 kpc corresponding to the extent of the region observed with the *Chandra* HETG of $\simeq 2$ arcsec, we then estimate a number density for the gas of $n_H \sim 0.5 \text{ cm}^{-3}$. The temperature, density and extension of the gas are indeed consistent with the values expected for the hot interstellar medium in giant elliptical galaxies

(Xu et al. 2002; Werner et al. 2009; Kim & Pellegrini 2012).

Evidence for an excess of emission in the *Chandra* image from 1 arcsec to 3 arcsec with respect to the point spread function reported in Ogle et al. (2005) is consistent with extended soft X-ray emission. We note that the resolving power of the grating may decrease if the source is extended. For instance, from Fig. 8.23 of the *Chandra* proposers guide³ we see that the MEG resolution could degrade down to $E/\Delta E \simeq 200$ for a 5 arcsec extended source at the wavelength of 17 Å. Therefore, at the energy of $E \simeq 700$ eV the resolution may degrade down to a worst value of 3.5 eV. However, we note that the observed emission line at $E \simeq 720$ eV listed in Table 2 is resolved with a width $\sigma = 8 \pm 2$ eV, which is at least twice larger than the worse energy resolution. Subtracting the 3.5 eV resolution in quadrature may only slightly reduce the broadening to around 7 eV, which is still consistent within the 1 sigma errors. Moreover, the same line, with consistent broadening, was reported also in the *XMM-Newton* RGS spectrum by Torresi et al. (2012). Thus, we are confident that the broadening of the line is not affected by the soft X-ray emission region possibly extending up to a few arcsecs.

The total X-ray luminosity between $E=0.1-10$ keV estimated for the hot gas in 3C 120 is $L_{hot} \simeq 1.5 \times 10^{42}$ erg s⁻¹. In order to keep the gas hot and prevent a catastrophic cooling flow, there must be some source of energy. An order of magnitude estimate of the cooling timescale for the hot gas associated with the galaxy can be estimated as $t_{cool} = U/L_{hot}$, where U is the internal energy of the gas defined as $U = (3/2)NkT$, where N is the number of particles and T is the temperature. For an estimated density of $n \simeq 0.5$ cm⁻³ and considering a spherical region of radius about 1.3 kpc and temperature $T \simeq 10^7$ K, we derive $U \simeq 6 \times 10^{55}$ ergs. We can then estimate a short cooling time of the order of ~ 1 Myr or up to ~ 10 Myr using the prescription in Peterson & Fabian (2006). Therefore, either most of the gas was heated more recently than this time-scale or there is an additional source of heating that keeps it hot.

Shocks or outbursts can disturb the typical collisional plasma found in the galactic interstellar medium. The spectrum emitted by this plasma contains diagnostics that have been used to determine the time since the disturbing event, although this determination becomes uncertain as the elements return to equilibrium. For instance, this method has been used to determine the age of supernova remnants or to determine when individual knots in the ejecta were shocked (e.g., Hwang & Laming

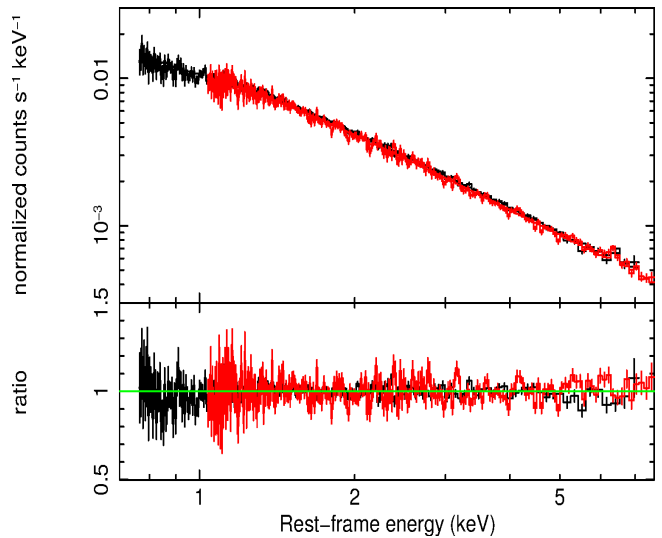


Figure 4. Combined *Chandra* MEG (black) and HEG (red) spectra of 3C 120 compared with the best-fit model. *Upper panel:* spectra and continuum model, the data are divided by the response effective area for each channel. *Lower panel:* data to model ratio. The data are binned to $4 \times$ the FWHM resolution and to a minimum signal-to-noise of 5 for clarity.

2003; Yatsu et al. 2005).

From our best-fit with a non-equilibrium ionization model we estimate an ionization timescale of $\tau = (1.3^{+1.2}_{-1.0}) \times 10^{11}$ s cm⁻³. Figure 1 in Smith & Hughes (2010) show the typical timescales of different ions to reach equilibrium for different temperatures. For a temperature of $T \simeq 10^7$ K estimated here from the Fe L emission lines we see that a characteristic time-scale to reach 90% of equilibrium would be much longer, of $\tau \simeq 9 \times 10^{11}$ s cm⁻³. Therefore, the observed gas is about a factor of seven in time away from reaching equilibrium.

Considering the indicative number density of $n \simeq 0.5$ cm⁻³, we obtain a timescale of $\sim 10^{11}$ s or about 10,000 years since the main disturbance of the gas occurred. It is tempting to relate such time-scale with the onset or with intermittent outburst activity of the powerful jet or winds in this AGN, perhaps in line with evolutionary scenarios (Reynolds & Begelman 1997; Czerny et al. 2009; Baldi et al. 2015). This scenario is also consistent with the possible thermal emission from isothermal shocks suggested by Halpern et al. (1985) as an explanation of the continuum emission and variability of 3C 120 using data from the *Einstein* X-ray observatory. The shocks in Halpern et al. (1985) have higher density, velocity ($v_s \sim 20,000$ km s⁻¹), and temperature ($kT \sim 7 \times 10^7$ K), and are located closer to the black hole (at \sim pc scales) compared to the ones observed through Fe L line emission here and in Petre et al. (1984). In analogy to supernova remnants, this may indicate a superposition or stratification of AGN shocks with various locations and ages.

³ http://cxc.cfa.harvard.edu/proposer/POG/html/chap8.html#tth_sEc8.2

Further support for the hot gas being heated by AGN driven shocks comes also from the comparison of the warm mid-IR H_2 emission compared to the thermal emission in radio galaxies. In particular, Ogle et al. (2010) detected the H_2 S(1) line in 3C 120, suggesting that the most likely heating mechanism is jet-driven shocks in a multiphase interstellar medium. Moreover, Lanz et al. (2015) reported a similar luminosity in the midIR H_2 lines and in the thermal X-ray emission for radio galaxies whose midIR spectrum indicates the presence of shocks.

These evidences, together with the large velocity broadening of the hot emission component in 3C 120 of about $1,000 \text{ km s}^{-1}$ point to the possibility that the velocity width could be due to a spherical outflow or an expanding spherical shocked bubble, perhaps driven by the winds or jet from the central AGN. We note that the Fermi bubbles observed in our Milky Way have indeed a comparable temperature and size, and they are estimated to be expanding with a shock speed of $v_{shock} \simeq 1,000 \text{ km s}^{-1}$ (Fox et al. 2015; Nicastro et al. 2016).

We note that 3C 120 shows both ultrafast outflows and radio jets with powers of $P_{UFO} \sim 1 \times 10^{44} \text{ erg s}^{-1}$ and $P_{jet} \sim 5 \times 10^{44} \text{ erg s}^{-1}$, respectively (Tombesi et al. 2010b, 2014; Torresi et al. 2012). Hot shocked bubble are indeed expected from theory of AGN feedback driven by winds or jets (e.g., Wagner et al. 2012, 2013; Zubovas & Nayakshin 2014). As the AGN wind sweeps up the ambient medium the forward shock decelerates producing cooler gas with a temperature of $T \simeq 10^7 \text{ K}$ for a shock velocity of $v_{shock} \simeq 1,000 \text{ km s}^{-1}$. Momentum conservation implies that the mean density swept up by the AGN wind is then of the order of $n \simeq 0.1 \text{ cm}^{-3}$ for an AGN luminosity of $L \sim 10^{45} \text{ erg s}^{-1}$, a shock radius of $R_s \sim 1 \text{ kpc}$ and velocity of $v_{shock} \sim 1,000 \text{ km s}^{-1}$. The typical X-ray luminosity of such wind shocked gas from bremsstrahlung would be of $L_X \sim 10^{42} \text{ erg s}^{-1}$ (Bourne & Nayakshin 2013; Nims et al. 2015). These parameters are indeed consistent with the estimates for the hot X-ray emitting gas in 3C 120.

A possible variability of the emitter was reported by Petre et al. (1984). Torresi et al. (2012) reported the following parameters for the emission line in the *XMM-Newton* RGS spectrum of 3C 120 obtained in 2003: line energy of $E \sim 730 \text{ eV}$, flux of $I \simeq 7 \times 10^{-5} \text{ ph s}^{-1} \text{ cm}^{-2}$, and line width FWHM=4,800 $^{+2,300}_{-2,700} \text{ km s}^{-1}$. Comparing to the parameters of the emission line in our *Chandra* HETG spectrum reported in Table 2, we note that the main difference in the 11 years spanning between the two observations is a factor of three increase in line flux. In the framework of a hot shocked bubble, we would expect an increase in X-ray bremsstrahlung luminosity as the wind shock expands to larger radii (e.g., Nims et

al. 2015). Future high-energy resolution observations of the source may confirm this scenario.

On the other hand, we note that the X-ray emission expected from star formation can be estimated as $L_{x(0.5-8keV)} \simeq 4 \times 10^{39} (\dot{M}_*/1M_\odot \text{ yr}^{-1}) \text{ erg s}^{-1}$, with a scatter of $\simeq 0.4 \text{ dex}$, where \dot{M}_* is the star formation rate (Mineo et al. 2014). Given the star formation rate in 3C 120 of $\dot{M}_* = 2.8^{+0.9}_{-1.0} M_\odot \text{ yr}^{-1}$ estimated by Westhues et al. (2016) using multiwavelength data, the resultant X-ray luminosity would be orders of magnitude lower than observed.

The radio galaxy 3C 120 is an isolated, peculiar S0 galaxy about 25 kpc in diameter. The optical appearance is complex, with multiple dust lanes and two suggestive spiral arms that become radial features at a projected distance of about 6.3 kpc from the core. It is not clear whether the peculiar optical morphology, perturbed rotation curve and wide-spread enhanced star formation are due to the effects of tidal perturbation or interaction of the radio jet with the galaxy (Harris et al. 2004). It has been suggested that the optical data indicate a merger which is near completion (Heckman et al. 1986; Moles et al. 1988).

Indeed, integral field spectroscopy of the central regions of 3C 120 shows evidence of shells in the central kpc region that may be remnants of a past merging event in this galaxy and/or interaction of the radio jet with the intergalactic medium (Garcia-Lorenzo et al. 2005). 3C 120 is a bulge-dominated galaxy that has, most probably, experienced a merging event with a less massive galaxy. That galaxy was completely disrupted in the merging process, falling in parts that produce, most probably, many of the observed optical structures. There is also evidence that a substantial fraction of its gas has been channeled toward the inner regions, perhaps activating a new feeding phase for the central supermassive black hole (Garcia-Lorenzo et al. 2005).

Indeed, CO emission data add substantial support to the hypothesis that 3C 120 involves a merger of gas-rich galaxies. The CO line profile is broad with FWHM=500 km s^{-1} and full width at zero intensity (FWZI) of 710 km s^{-1} (Mazzarella et al. 1993; Evans et al. 2005). The velocity broadening is probably dominated by rotation, but there is also a component coming from disturbances due to the radio jet or AGN wind. The estimated H_2 mass is large, $\log M(H_2) = 9.79 M_\odot$. This corresponds to about twice the molecular gas content of the Milky Way. These CO data corroborate evidence from optical imaging that this and similar radio galaxies originate in collisions and mergers between disk galaxies, as recently suggested also by other authors (e.g., Chiaberge et al. 2015).

Combined radio, optical and *Chandra* X-ray images

show complex interactions and shocks between the radio jet and colder material. Harris et al. (2004) showed that the radio jet may be impacting a cold, spiral-like structure observable at 4 arcsec (about 2.5 kpc) from the nucleus. A bright radio, X-ray and optical jet knot emission is observed at this location (Harris et al. 2004). Evidence for complex mixing between hot shocked gas and cold gas due to the interaction between AGN winds or jets has been recently reported in an increasing number of sources (e.g., Morganti et al. 2013; Tadhunter et al. 2014; Tombesi et al. 2015; Feruglio et al. 2015; Dasyra et al. 2016). All these characteristics may place 3C 120 in a comparable parameter space of the AGN dominated ULIRGs (Veilleux et al. 2013; Cicone et al. 2014).

3.2. Lack of a warm absorber

We do not detect any significant ionized absorption feature in the soft X-rays. This is consistent with previous studies using *XMM-Newton* RGS (Ogle et al. 2005; Torresi et al. 2012) and a shorter *Chandra* HETG (McKernan et al. 2007). Using an *xstar* photo-ionized absorption table and assuming the typical ionization of the WA detected in other BLRGs of $\log\xi \simeq 2.5$ erg s⁻¹ cm and a velocity consistent with zero at the source rest-frame (Reeves et al. 2009; Torresi et al. 2010, 2012), we estimate a very low upper limit of the column density of a possible WA of just $N_H < 5 \times 10^{19}$ cm⁻².

From the previous discussion of hot emission in the soft X-rays, we suggest that the lack of a warm absorber may be due to the fact that the temperature of the hot interstellar medium of $T \sim 10^7$ K is much higher than the typical one for warm absorbers of $T \sim 10^5$ K (Chakravorty et al. 2009). Therefore, it is plausible that the warm absorbing gas often observed in Seyfert galaxies, if present, has been heated up too much and it is not observable.

3.3. Fe K emission and absorption

The Fe K band spectrum of 3C 120 in Fig. 2 is very rich, showing a series of at least four narrow emission and absorption lines due to iron at different ionization states. An unresolved Fe K α emission line at $E \simeq 6.39$ keV, an associated Compton shoulder at $E \simeq 6.23$ keV and the Fe K β at $E \simeq 7.05$ keV from cold or neutral gas.

The Fe K α emission line is unresolved, with a FWHM of less than 2,300 km s⁻¹, consistent with previous estimates (Yaqoob et al. 2004; Shu et al. 2010). This value is comparable to the width of the core of the broad line region (BLR) observed in optical H α and H β lines (Kollatschny et al. 2014), possibly suggesting a spatial overlap between the cold X-ray material and optical line emitting gas. The narrowness of the line may be also

consistent with the low inclination observed from the radio jet of 20° (Jorstad et al. 2005).

It is interesting to note that although the FWHM of the H α /H β lines is about 2,000 km s⁻¹, the FWZI calculated considering the width of the line at which it reaches the continuum level is much larger, reaching velocities of up to 15,000 km s⁻¹ (Phillips & Osterbrock 1975; Osterbrock 1977). The large difference between the FWHM and the FWZI indicates that the lines should have broad and complex wings. The FWZI is indeed more representative of the full range of velocities in the BLR. Such broad wings could possibly be associated with the part of the BLR closer to the black hole if due to rotation and/or to a possible fast bipolar outflow component. If the Fe K α at $E \simeq 6.4$ keV is related to the BLR, then it may show similar broad wings. However, the signal-to-noise of the current *Chandra* HETG observation is not high enough to test this possibility.

A detailed characterization using models of X-ray reflection from cold material gives a low reflection fraction of $R = 0.22 \pm 0.04$ consistent with the relatively low EW of the Fe K α emission line of $EW = 32 \pm 6$ eV. The column density of the torus is estimated to be Compton-thick, with $N_H > 6 \times 10^{24}$ cm⁻² in the equatorial plane if the *MYTorus* geometry is assumed. The detection of a Compton shoulder to the main Fe K α line is consistent with these estimates (Awaki et al. 2008). The overall low reflection fraction may indicate a clumpy torus outside the line of sight or a high opening angle of the reflecting material (e.g., Tazaki et al. 2013).

Comparing the extrapolated $E = 2-10$ keV X-ray luminosity of $L_{2-10} \simeq 1.4 \times 10^{44}$ erg s⁻¹ and $EW = 32 \pm 6$ eV derived here for 3C 120 with the Fig. 7 in Ricci et al. (2013) we see that the values for this radio galaxy are consistent with those expected in the range between Seyferts and quasars. This is consistent with the X-ray Baldwin effect, which would relate the decrease of the covering factor of the torus with the increase in luminosity (e.g., Iwasawa & Taniguchi 1993).

The shape and strength of the neutral Fe K α emission line suggest that the material feeding the accretion disk, or the torus, may be in the form of Compton-thick, clumpy clouds in an equatorial distribution. This is consistent with a recent model linking the micro and macro properties of AGN feeding and feedback (Gaspari & Sadowski 2017). In this model the inflow occurs via chaotic cold accretion, in which a rain of cold clouds condensing out of the quenched cooling flow is recurrently funneled via inelastic collisions. At the accretion disk scales, the accretion energy is transformed into ultrafast outflows and jets, ejecting most of the inflowing mass. The relatively high Eddington ratio of 3C 120 of $L/L_{Edd} \sim 0.3$ is also consistent with the accretion disk being mostly relatively cold and efficient, with episodic

thermal or magnetic instabilities linked to jet ejection events (Chatterjee et al. 2009; Tombesi et al. 2010; Lohfink et al. 2013).

Besides emission and reflection from cold material, an Fe XXV He α emission line at $E \simeq 6.7$ keV is also indicative of the presence of a significant amount of highly ionized gas in the central regions of this source. From the photoionization modeling we derive an ionization parameter of $\log \xi = 3.75^{+0.27}_{-0.38}$ erg s $^{-1}$ cm and a column density of $N_H > 1 \times 10^{22}$ cm $^{-2}$. From the definition of the ionization parameter, and assuming a compact spherical shell distribution ($\Delta R/R \leq 1$), we can estimate an upper limit on the distance of the emitting material from the X-ray source as $R_{max} = L_{ion}/\xi N_H$ (e.g., Tombesi et al. 2013a; Gofford et al. 2015). Substituting the estimated column density, ionization parameter, and ionizing luminosity, we derive the upper limit of $\simeq 2$ pc.

Absorption residuals in the energy range $E \simeq 7.2$ – 7.4 keV are suggestive of a possible ultrafast outflow with mildly relativistic velocity of $v_{out} = 0.068 \pm 0.002c$, a high ionization parameter $\log \xi = 3.48^{+0.17}_{-0.10}$ erg s $^{-1}$ cm, and a column density of $N_H = (3.3^{+2.4}_{-1.6}) \times 10^{21}$ cm $^{-2}$. These parameters are consistent with the ultrafast outflow detected in a previous 2006 *Suzaku* observation (Tombesi et al. 2010b, 2014). Considering the previous formula for R_{max} used for the ionized emitter, and substituting the parameters estimated from the fit, we can derive an upper limit of the distance of the absorber from the X-ray source of less than $\simeq 10$ pc.

Interestingly, the ionization parameter, column density, and distance of the Fe XXV emitter and the ultrafast outflow are comparable, suggesting the possibility that the ionized emission and absorption may originate from the same or related material. Therefore, we may be observing emission and absorption from the same extended outflow, as evinced also from *Suzaku* observations of another radio galaxy, namely 3C 111 (Tombesi et al. 2013b).

An intriguing phenomenon detected in a number of radio imaging observations of AGN jets in blazars and some radio galaxies, notably 3C 120, is the presence of transverse gradients in the Faraday rotation across the jet at parsec scales (Gómez et al. 2000, 2008, 2011). The origin and nature of such Faraday screen is still debated. It may be linked to the jet itself, such as a jet sheath with an helical/toroidal magnetic field (e.g., Gabuzda et al. 2014), or to magnetized gaseous clouds completely external to the jet (e.g., Zavala & Taylor 2004). In the case of 3C 120, the Faraday screen has been linked to a clumpy sheath of thermal electrons surrounding the radio jet and interacting with the jet at the de-projected distance of 8 pc, with a hydrogen equivalent column density of $N_H \sim 6 \times 10^{22}$ cm $^{-2}$ (Gómez et al. 2000, 2008). The fact that the observed changes in the polarization

properties of the underlying jet emission and in the rotation measure seem uncorrelated implies that the Faraday screen and the jet are likely not closely physically related. At the same time, sign reversals in the rotation measure along the jet observed on the time scale of a few/several years imply that the Faraday screen medium is at least mildly relativistic (Gómez et al. 2011).

It is interesting to consider that the ionized emission/absorption components observed in the Fe K band may be linked to the Faraday screen seen in radio. In fact, the column density, distance and relatively large outflow velocity of $v_{out} \simeq 0.07 c$ are consistent with this possibility and they could naturally explain the observed rotation measure variability (Zavala & Taylor 2004).

4. CONCLUSIONS

We reported the spectral analysis of a long 200 ks *Chandra* HETG observation of the radio galaxy 3C 120. The spectrum shows complex emission and absorption features in the soft X-rays and the Fe K band. We detect a neutral Fe K α line and accompanying emission lines indicative of a Compton-thick cold reflector with low reflection fraction, possibly due to a large opening angle of the torus. We observe also a highly ionized Fe XXV emission feature and possible evidence for a highly ionized disk wind consistent with previous claims. We do not find evidence for a warm absorber, which may instead be replaced by a hot emitting gas with temperature $kT \simeq 0.7$ keV observed as soft X-ray emission from ionized Fe L-shell lines which may originate from a kpc scale shocked bubble inflated by the AGN wind or jet with a shock velocity of about 1,000 km s $^{-1}$. This dataset shows the wealth of information that can be derived from high energy resolution X-ray spectroscopy and it will be very interesting to compare to other multi-wavelength observations to explore the multi-phase and multi-scale structure of AGN feeding and feedback of powerful radio galaxies. In particular, deeper X-ray observations with high energy resolution spectrometers will be fundamental to constrain the accretion onto and the ejection from the central supermassive black hole and deeper mm or IR observations will allow to investigate the connection with the large reservoir molecular gas.

F.T. thanks M. Elvis, R. Petre, and S. Veilleux for the useful discussions. F.T. and C.S.R. acknowledges support for this work by the National Aeronautics and Space Administration (NASA) through Chandra Award Number GO4-15103A issued by the Chandra X-ray Observatory Center, which is operated by the Smithsonian Astrophysical Observatory for and on behalf of NASA under contract NAS8-03060. C.S.R. acknowledges support from the NASA ASTRO-H grant NNX15AU54G.

L. S. was supported by the Polish National Science Centre through the grant DEC2012/04/A/ST9/00083.

REFERENCES

- Asplund, M., Grevesse, N., Sauval, A. J., & Scott, P. 2009, *ARA&A*, 47, 481
- Awaki, H., Anabuki, N., Fukazawa, Y., et al. 2008, *PASJ*, 60, S293
- Baldi, R. D., Capetti, A., & Giovannini, G. 2015, *A&A*, 576, A38
- Ballantyne, D. R. 2005, *MNRAS*, 362, 1183
- Ballo, L., Braitto, V., Reeves, J. N., Sambruna, R. M., & Tombesi, F. 2011, *MNRAS*, 418, 2367
- Bostrom, A., Reynolds, C. S., & Tombesi, F. 2014, *ApJ*, 791, 119
- Borkowski, K. J., Lyerly, W. J., & Reynolds, S. P. 2001, *ApJ*, 548, 820
- Bourne, M. A., & Nayakshin, S. 2013, *MNRAS*, 436, 2346
- Braitto, V., Reeves, J. N., Sambruna, R. M., & Gofford, J. 2011, *MNRAS*, 414, 2739
- Cicone, C., Maiolino, R., Sturm, E., et al. 2014, *A&A*, 562, A21
- Chatterjee, R., Marscher, A. P., Jorstad, S. G., et al. 2009, *ApJ*, 704, 1689
- Chatterjee, R., Marscher, A. P., Jorstad, S. G., et al. 2011, *ApJ*, 734, 43
- Chakravorty, S., Kembhavi, A. K., Elvis, M., & Ferland, G. 2009, *MNRAS*, 393, 83
- Chiaberge, M., Gilli, R., Lotz, J. M., & Norman, C. 2015, *ApJ*, 806, 147
- Claudice, D., Perlman, E. S., Georganopoulos, M., et al. 2016, *ApJ*, 826, 109
- Croton, D. J., Springel, V., White, S. D. M., et al. 2006, *MNRAS*, 365, 11
- Czerny, B., Siemiginowska, A., Janiuk, A., Nikiel-Wroczyński, B., & Stawarz, L. 2009, *ApJ*, 698, 840
- Dasyra, K. M., Combes, F., Oosterloo, T., et al. 2016, *A&A*, 595, L7
- Evans, A. S., Mazzarella, J. M., Surace, J. A., et al. 2005, *ApJS*, 159, 197
- Fabian, A. C. 1999, *MNRAS*, 308, L39
- Fabian, A. C. 2012, *ARA&A*, 50, 455
- Gabuzda, D. C., Reichstein, A. R., & O'Neill, E. L. 2014, *MNRAS*, 444, 172
- García, J., Dauser, T., Lohfink, A., et al. 2014, *ApJ*, 782, 76
- García-Lorenzo, B., Sánchez, S. F., Mediavilla, E., González-Serrano, J. I., & Christensen, L. 2005, *ApJ*, 621, 146
- Garofalo, D., Evans, D. A., & Sambruna, R. M. 2010, *MNRAS*, 406, 975
- Gaspari, M., & Sadowski, A. 2017, arXiv:1701.07030
- George, I. M., & Fabian, A. C. 1991, *MNRAS*, 249, 352
- Gofford, J., Reeves, J. N., Tombesi, F., et al. 2013, *MNRAS*, 430, 60
- Gofford, J., Reeves, J. N., McLaughlin, D. E., et al. 2015, *MNRAS*, 451, 4169
- Gómez, J.-L., Marscher, A. P., Alberdi, A., Jorstad, S. G., & García-Miró, C. 2000, *Science*, 289, 2317
- Gómez, J. L., Marscher, A. P., Jorstad, S. G., Agudo, I., & Roca-Sogorb, M. 2008, *ApJL*, 681, L69
- Gómez, J. L., Roca-Sogorb, M., Agudo, I., Marscher, A. P., & Jorstad, S. G. 2011, *ApJ*, 733, 11
- Halpern, J. P. 1985, *ApJ*, 290, 130
- Hardcastle, M. J., Evans, D. A., & Croston, J. H. 2009, *MNRAS*, 396, 1929
- Harris, D. E., Mossman, A. E., & Walker, R. C. 2004, *ApJ*, 615, 161
- Heckman, T. M., Smith, E. P., Baum, S. A., et al. 1986, *ApJ*, 311, 526
- Hopkins, P. F., Hernquist, L., Cox, T. J., & Kereš, D. 2008, *ApJS*, 175, 356-389
- Hughes, S. A., & Blandford, R. D. 2003, *ApJL*, 585, L101
- Hwang, U., & Laming, J. M. 2003, *ApJ*, 597, 362
- Ikeda, S., Awaki, H., & Terashima, Y. 2009, *ApJ*, 692, 608
- Iwasawa, K., & Taniguchi, Y. 1993, *ApJL*, 413, L15
- Feruglio, C., Fiore, F., Carniani, S., et al. 2015, *A&A*, 583, A99
- Fukumura, K., Tombesi, F., Kazanas, D., et al. 2014, *ApJ*, 780, 120
- Fox, A. J., Bordoloi, R., Savage, B. D., et al. 2015, *ApJL*, 799, L7
- Jorstad, S. G., Marscher, A. P., Lister, M. L., et al. 2005, *AJ*, 130, 1418
- Kalberla, P. M. W., Burton, W. B., Hartmann, D., et al. 2005, *A&A*, 440, 775
- Kallman, T., & Bautista, M. 2001, *ApJS*, 133, 221
- Kataoka, J., Reeves, J. N., Iwasawa, K., et al. 2007, *PASJ*, 59, 279
- Kataoka, J., Stawarz, L., Takahashi, Y., et al. 2011, *ApJ*, 740, 29
- Kim, D.-W., & Pellegrini, S. 2012, *Astrophysics and Space Science Library*, 378,
- King, A., & Pounds, K. 2015, *ARA&A*, 53, 115
- Kollatschny, W., Ulbrich, K., Zetzl, M., Kaspi, S., & Haas, M. 2014, *A&A*, 566, A106
- Lanz, L., Ogle, P. M., Evans, D., et al. 2015, *ApJ*, 801, 17
- Liedahl, D. A., & Paerels, F. 1996, *ApJL*, 468, L33
- Lohfink, A. M., Reynolds, C. S., Jorstad, S. G., et al. 2013, *ApJ*, 772, 83
- Lohfink, A. M., Ogle, P., Tombesi, F., et al. 2015, *ApJ*, 814, 24
- Marscher, A. P., Jorstad, S. G., Gómez, J.-L., et al. 2002, *Nature*, 417, 625
- Matt, G. 2002, *MNRAS*, 337, 147
- Mazzarella, J. M., Graham, J. R., Sanders, D. B., & Djorgovski, S. 1993, *ApJ*, 409, 170
- McKernan, B., Yaqoob, T., & Reynolds, C. S. 2007, *MNRAS*, 379, 1359
- Mineo, S., Gilfanov, M., Lehmer, B. D., Morrison, G. E., & Sunyaev, R. 2014, *MNRAS*, 437, 1698
- Moles, M., del Olmo, A., Masegosa, J., & Perea, J. D. 1988, *A&A*, 197, 1
- Morganti, R., Fogasy, J., Paragi, Z., Oosterloo, T., & Orienti, M. 2013, *Science*, 341, 1082
- Murphy, K. D., & Yaqoob, T. 2009, *MNRAS*, 397, 1549
- Nandra, K., O'Neill, P. M., George, I. M., & Reeves, J. N. 2007, *MNRAS*, 382, 194
- Nicastro, F., Senatore, F., Krongold, Y., Mathur, S., & Elvis, M. 2016, *ApJL*, 828, L12
- Nims, J., Quataert, E., & Faucher-Giguère, C.-A. 2015, *MNRAS*, 447, 3612
- Ogle, P. M., Davis, S. W., Antonucci, R. R. J., et al. 2005, *ApJ*, 618, 139
- Ogle, P., Boulanger, F., Guillard, P., et al. 2010, *ApJ*, 724, 1193
- Osterbrock, D. E. 1977, *ApJ*, 215, 733
- Peterson, J. R., & Fabian, A. C. 2006, *PhR*, 427, 1
- Petre, R., Mushotzky, R. F., Holt, S. S., & Krolik, J. H. 1984, *ApJ*, 280, 499
- Phillips, M. M., & Osterbrock, D. E. 1975, *PASP*, 87, 949
- Reeves, J. N., Sambruna, R. M., Braitto, V., & Eracleous, M. 2009, *ApJL*, 702, L187
- Reeves, J. N., Gofford, J., Braitto, V., & Sambruna, R. 2010, *ApJ*, 725, 803
- Reynolds, C. S., & Begelman, M. C. 1997, *ApJL*, 487, L135

- Reynolds, C. S., Lohfink, A. M., Ogle, P. M., et al. 2015, *ApJ*, 808, 154
- Ricci, C., Paltani, S., Awaki, H., et al. 2013, *A&A*, 553, A29
- Sambruna, R. M., Reeves, J. N., Braitto, V., et al. 2009, *ApJ*, 700, 1473
- Shu, X. W., Yaqoob, T., & Wang, J. X. 2010, *ApJS*, 187, 581
- Sikora, M., Stawarz, L., & Lasota, J.-P. 2007, *ApJ*, 658, 815
- Sikora, M., & Begelman, M. C. 2013, *ApJL*, 764, L24
- Silk, J., & Rees, M. J. 1998, *A&A*, 331, L1
- Smith, R. K., Brickhouse, N. S., Liedahl, D. A., & Raymond, J. C. 2001, *ApJL*, 556, L91
- Smith, R. K., & Hughes, J. P. 2010, *ApJ*, 718, 583
- Springel, V., Di Matteo, T., & Hernquist, L. 2005, *ApJL*, 620, L79
- Tadhunter, C., Morganti, R., Rose, M., Oonk, J. B. R., & Oosterloo, T. 2014, *Nature*, 511, 440
- Tarter, C. B., Tucker, W. H., & Salpeter, E. E. 1969, *ApJ*, 156, 943
- Tazaki, F., Ueda, Y., Terashima, Y., Mushotzky, R. F., & Tombesi, F. 2013, *ApJ*, 772, 38
- Tchekhovskoy, A., Narayan, R., & McKinney, J. C. 2010, *ApJ*, 711, 50
- Tchekhovskoy, A., Narayan, R., & McKinney, J. C. 2011, *MNRAS*, 418, L79
- Tombesi, F., Cappi, M., Reeves, J. N., et al. 2010a, *A&A*, 521, A57
- Tombesi, F., Sambruna, R. M., Reeves, J. N., et al. 2010b, *ApJ*, 719, 700
- Tombesi, F., Sambruna, R. M., Reeves, J. N., Reynolds, C. S., & Braitto, V. 2011, *MNRAS*, 418, L89
- Tombesi, F., Cappi, M., Reeves, J. N., & Braitto, V. 2012a, *MNRAS*, 422, 1
- Tombesi, F., Sambruna, R. M., Marscher, A. P., et al. 2012b, *MNRAS*, 424, 754
- Tombesi, F., Cappi, M., Reeves, J. N., et al. 2013a, *MNRAS*, 430, 1102
- Tombesi, F., Reeves, J. N., Reynolds, C. S., García, J., & Lohfink, A. 2013b, *MNRAS*, 434, 2707
- Tombesi, F., Tazaki, F., Mushotzky, R. F., et al. 2014, *MNRAS*, 443, 2154
- Tombesi, F., Meléndez, M., Veilleux, S., et al. 2015, *Nature*, 519, 436
- Tombesi, F., Reeves, J. N., Kallman, T., et al. 2016, *ApJ*, 830, 98
- Torresi, E., Grandi, P., Longinotti, A. L., et al. 2010, *MNRAS*, 401, L10
- Torresi, E., Grandi, P., Costantini, E., & Palumbo, G. G. C. 2012, *MNRAS*, 419, 321
- Veilleux, S., Meléndez, M., Sturm, E., et al. 2013, *ApJ*, 776, 27
- Verner, D. A., Verner, E. M., & Ferland, G. J. 1996, *Atomic Data and Nuclear Data Tables*, 64, 1
- Wagner, A. Y., Bicknell, G. V., & Umemura, M. 2012, *ApJ*, 757, 136
- Wagner, A. Y., Umemura, M., & Bicknell, G. V. 2013, *ApJL*, 763, L18
- Watanabe, M., Nagata, T., Sato, S., Nakaya, H., & Hough, J. H. 2003, *ApJ*, 591, 714
- Werner, N., Zhuravleva, I., Churazov, E., et al. 2009, *MNRAS*, 398, 23
- Westhues, C., Haas, M., Barthel, P., et al. 2016, *AJ*, 151, 120
- Wilson, A. S., & Colbert, E. J. M. 1995, *ApJ*, 438, 62
- Xu, C., Livio, M., & Baum, S. 1999, *AJ*, 118, 1169
- Xu, H., Kahn, S. M., Peterson, J. R., et al. 2002, *ApJ*, 579, 600
- Yaqoob, T., & Padmanabhan, U. 2004, *ApJ*, 604, 63
- Yaqoob, T., & Murphy, K. D. 2011, *MNRAS*, 412, 277
- Yatsu, Y., Kawai, N., Kataoka, J., et al. 2005, *ApJ*, 631, 312
- Zavala, R. T., & Taylor, G. B. 2004, *ApJ*, 612, 749
- Zubovas, K., & Nayakshin, S. 2014, *MNRAS*, 440, 2625